

## Electronic Supplementary Information (ESI)

### **All-in-one Ultrathin Nanoporous ZnIn<sub>2</sub>S<sub>4</sub> with Ameliorated Photoredox Capability: Harvesting Electron-hole Pairs in Cooperative Hydrogen and Benzaldehyde Production**

Grayson Zhi Sheng Ling,<sup>1,2</sup> Steven Hao Wan Kok,<sup>3</sup> Peipei Zhang,<sup>4</sup> Tan Ji Siang,<sup>1,2</sup> Choon Yian Haw,<sup>1,2,4</sup> Lling-Lling Tan,<sup>3</sup> Binghui Chen,<sup>1,2,4,5</sup> Wee-Jun Ong<sup>1,2,4,5,6,\*</sup>

<sup>1</sup>*School of Energy and Chemical Engineering, Xiamen University Malaysia, Sepang, Selangor Darul Ehsan, 43900, Malaysia*

<sup>2</sup>*Center of Excellence for NaNo Energy & Catalysis Technology (CONNECT), Xiamen University Malaysia, Sepang, Selangor Darul Ehsan, 43900, Malaysia*

<sup>3</sup>*Multidisciplinary Platform of Advanced Engineering, Chemical Engineering Discipline, School of Engineering, Monash University, Jalan Lagoon Selatan, Bandar Sunway, 47500 Selangor, Malaysia*

<sup>4</sup>*State Key Laboratory of Physical Chemistry of Solid Surfaces, College of Chemistry and Chemical Engineering, Xiamen University, Xiamen, 361005, China*

<sup>5</sup>*Gulei Innovation Institute, Xiamen University, Zhangzhou 363200, China*

<sup>6</sup>*Shenzhen Research Institute of Xiamen University, Shenzhen, 518057, China*

\*Corresponding author.

*E-mail: weejun.ong@xmu.edu.my; ongweejun@gmail.com*

*Homepage: <https://sites.google.com/site/wjongresearch/>*

## Supplementary Note 1 - Materials Characterization

The surface morphology images were obtained by field emission scanning electron microscopy (FESEM) using a Hitachi SU8010 microscope equipped with energy-dispersive X-ray (EDX), which is used to identify element distribution. High-resolution transmission electron microscopy (TEM/HRTEM) images were taken by JEOL JEM-2100F microscope equipped with 200 kV Field Emission (FE) analytical electron microscope. The thickness profile was acquired on a tapping mode-operated Bruker Multimode 8 atomic force microscope (AFM). Panalytical X'Pert Pro diffractometer with Cu K $\alpha$  radiation source was acquired to record XRD data at a step size of 0.02° from 5° to 80° (2 $\theta$ ). The Brunauer-Emmett-Teller (BET) surface area and Barrett, Joyner, and Halenda (BJH) pore distribution were measured through N<sub>2</sub> adsorption-desorption method at 77.40 K using Micrometrics ASAP 2020. 100 mg of sample was weighed and degassed at 120 °C for 12 h prior to the analysis. X-ray photoelectron spectroscopy (XPS) was acquired on Kratos AXIS Ultra DLD spectrometer using Al K $\alpha$  X-ray radiation of 1486.69 eV with calibration with respect to the C 1s peak at 284.6 eV. Jasco V-770 spectrophotometer was used to measure UV-Vis light absorption (200 <  $\lambda$  < 800 nm) with BaSO<sub>4</sub> as background reference. The Fourier transform infrared spectroscopy (FT-IR) spectra were examined by a PerkinElmer Spectrum Frontier FT-MIR spectrometer with a resolution of 8 cm<sup>-1</sup> using standard Attenuated total reflectance (ATR) technique. HORIBA LabRam HR Evolution Raman spectrometer was used to acquire Raman spectra at room temperature by using a 785 nm laser. Room temperature steady-state photoluminescence (PL) spectra were analyzed on the Raman spectrometer Horiba JY LabRAM HR Evolution using He-Cd laser under excitation wavelength of 325 nm. Zeta potentials were measured using an electrophoretic light scattering technique by Litesizer 500 with 658 nm laser at 15° angle. In-situ electron paramagnetic resonance (EPR) measurements were performed using a Bruker EMX-10/12 EPR spectrometer. To capture hydroxyl radicals, 5 mg photocatalyst was dispersed in 1 mL ultrapure water with 50  $\mu$ L 5,5-dimethyl-1-pyrroline-N-oxide (DMPO) under ultrasonication. Moreover, 2 mg sample was ultrasonically dispersed in 2 mL benzyl alcohol, and then 0.5 mL of the prepared suspension was mixed with 50  $\mu$ L DMPO for the test of carbon-centered (C $\alpha$ ) radical. Each of the first data points was collected in the dark, and the signal was collected at 10 min of light irradiation.

## Supplementary Note 2 - Photocatalytic dual-redox reaction

The photocatalytic hydrogen evolution coupled with benzyl alcohol oxidation was performed using a three-necked top-irradiation reactor cell. 20 mg of photocatalysts was dispersed in 60 mL deionized water with 0.6 mL benzyl alcohol and sonicated before irradiation. Subsequently, the suspension was bubbled with nitrogen gas through the reactor for 30 min to completely remove the air and dissolved oxygen and ensure that the reactor was in an anaerobic condition. The above suspension was irradiated under AM1.5 simulated sunlight filter using a 300 W Xenon lamp (CEL-PF300-T8, Beijing China Education Au-light (CEAuLight) Co., Ltd., 300 mW cm<sup>-2</sup>). The reaction temperature was maintained at room temperature using an external water bath. The amount of evolved hydrogen was monitored by an online Agilent GC 7890 gas chromatograph (GC) equipped with a thermal conductivity detector (TCD). After 4 h reaction, the supernatant liquid was obtained by centrifugation and separated from solid impurities using 0.22 μm nylon syringe filter. Benzaldehyde and its derivatives were quantified by high-performance liquid chromatography (Acquity Arc Waters HPLC system; column: Kinetex 2.6 μm Phenyl-Hexyl 100 Å; injection volume: 10 μL; mobile phase: water/acetonitrile = 60:40; column temperature: 40 °C; flow rate: 1 mL min<sup>-1</sup>; detector: Photodiode Array Detector (PDA) detection wavelength: 254 nm). Wavelength-dependent apparent quantum efficiency (AQE) was performed by repeating the above photocatalysis experiment with different band-pass filters of 380, 400, 420, 450, 500 and 550 nm and calculated based on the following equation,

$$AQE(\%) = 2 \times \frac{\text{Number of evolved } H_2 \text{ molecules}}{\text{Number of incident photons}} \times 100\% = \frac{2 \times \eta_{H_2}}{S \times P \times t} \times 100\%$$

where  $\eta_{H_2}$  is the total amount of H<sub>2</sub> evolved (mol), N<sub>A</sub> is Avogadro constant (6.02 × 10<sup>23</sup> mol<sup>-1</sup>), S is the irradiation area (33.18 cm<sup>2</sup>), P is the power intensity of light irradiation (W cm<sup>-2</sup>), t is the photoreaction time (14400 s), λ is the wavelength of the monochromatic light (nm), h is the Planck constant (6.626 × 10<sup>-34</sup> J s) and c is the speed of light (3 × 10<sup>8</sup> m s<sup>-1</sup>).

The obtained hydrogen evolution rate under AM.15 irradiation was further used to calculate solar-to-hydrogen (STH) efficiency according to the following equation:

$$STH(\%) = \frac{R_{H_2} \times \Delta G_{H_2}}{P \times S \times t} \times 100\%$$

Where  $R(H_2)$  is the  $H_2$  evolution rate ( $3.477 \times 10^{-4}$  mol) of 20 mg photocatalyst during 4 h photocatalysis,  $\Delta G$  is Gibbs free energy of the overall water splitting reaction ( $237130 \text{ J mol}^{-1}$ ),  $P$  is the energy intensity of the AM 1.5G solar light irradiation ( $0.0846 \text{ W cm}^{-2}$ ),  $S$  is the irradiation area ( $33.18 \text{ cm}^2$ ) and  $t$  is the irradiation time (14400 s)

Control experiments were performed without light irradiation or in the absence of photocatalyst. Another control experiment was conducted by replacing water with acetonitrile as the reaction medium. Radical experiments were performed using different scavengers, where the scavengers were added the same as the mole of benzyl alcohol in the solution. For the prolonged stability test, the optimal photocatalyst was continuously irradiated for 12 h without replacing the original solvent and replenishing benzyl alcohol.

### Supplementary Note 3 - Photoelectrochemical measurement

Electrochemical impedance spectroscopy (EIS), Mott-Schottky (M-S), linear sweep voltammetry (LSV) and transient photocurrent responses tests were performed on a Metrohm Autolab (PGSTAT204) electrochemical workstation. All photoelectrochemical measurements were conducted using a typical three-electrode system, where Ag/AgCl, Pt sheet and photocatalyst-coated thin film were employed as the reference, counter and working electrode, respectively in 0.1 M  $Na_2SO_4$  electrolyte solution. For the working electrode preparation, 10 mg catalyst, 40  $\mu\text{L}$  Nafion and 300  $\mu\text{L}$  ethanol were stirred overnight and 40  $\mu\text{L}$  of the suspension was drop-casted onto FTO glass with a square area of  $1 \text{ cm}^2$ . EIS was measured under open-circuit voltage with frequencies range between 0.01 and  $1 \times 10^5$  Hz and AC amplitude of 0.01 V under dark and light on conditions (15 cm-away AM 1.5 light irradiation). Mott-Schottky plots were taken at AC frequencies of 0.5, 0.75, and 1 kHz. The density charge carrier based on Mott-Schottky slope was calculated as follows:

$$N_D = \frac{2}{\epsilon\epsilon_0 e} \frac{dV}{d\frac{1}{C^2}} = \frac{2}{\epsilon\epsilon_0 e} \frac{1}{slope}$$

where  $N_D$  is the charge density of semiconductors,  $\epsilon$  is the dielectric constant of  $ZnIn_2S_4$  (21.62),  $\epsilon_0$  is the vacuum permittivity ( $8.85 \times 10^{-14} \text{ F cm}^{-2}$ ) and  $e$  is the electronic charge ( $1.6 \times 10^{-19} \text{ C}$ ). The measured potential vs. Ag/AgCl was converted to the normal hydrogen electrode (NHE) scale with the Nernst equation:  $E_{NHE} = E_{Ag/AgCl} + 0.059 \times \text{pH} + E^0$ , where  $E^0(\text{Ag/AgCl}) = 0.197 \text{ V}$  at  $25 \text{ }^\circ\text{C}$ . The LSV measurements were tested at a scan rate of 0.01 V

s<sup>-1</sup> with step size of 0.002 V. Transient photocurrent responses were examined with 15 cm-away AM1.5 light irradiation every 30 s light on/off time interval at 0.5 V vs. Ag/AgCl.

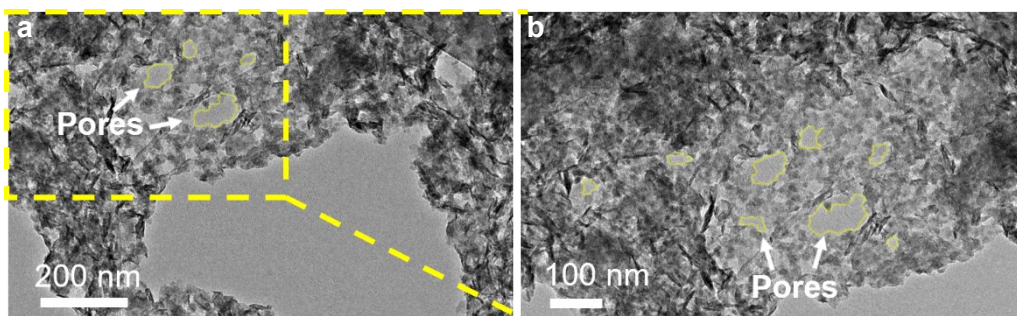


**Fig. S1** TEM images of LZIS-4.

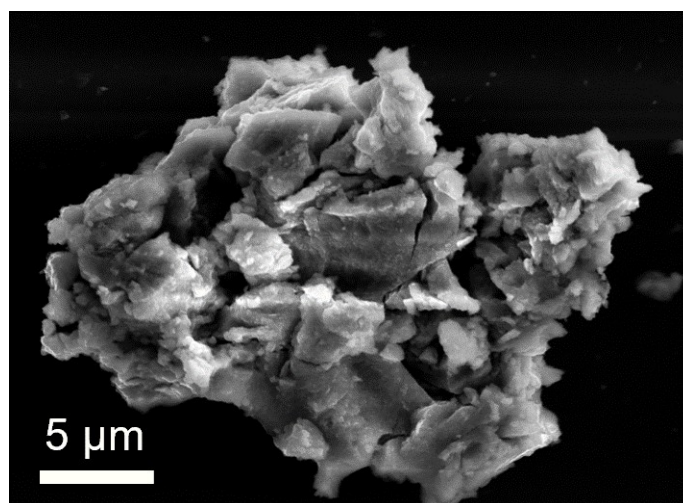


**Fig. S2** FESEM image of aggregated LZIS-6 with 600 mg trisodium citrate modification.

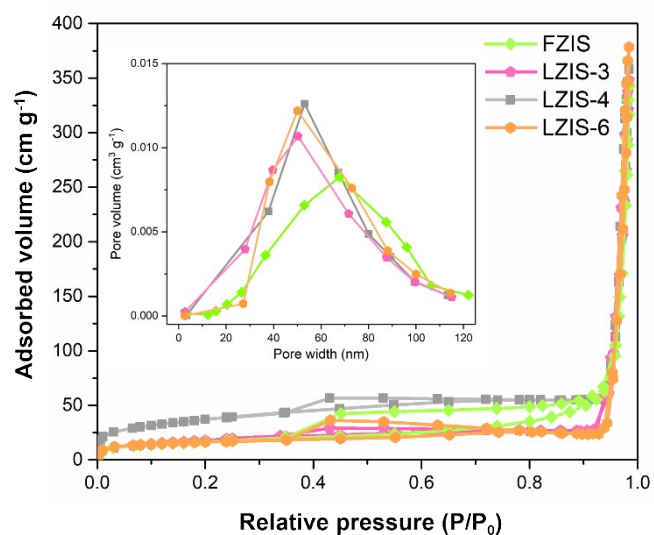


**Fig. S3** N<sub>2</sub> adsorption-desorption isotherms and BJH pore distribution (inset) of FZIS, LZIS-3, LZIS-4 and LZIS-6.

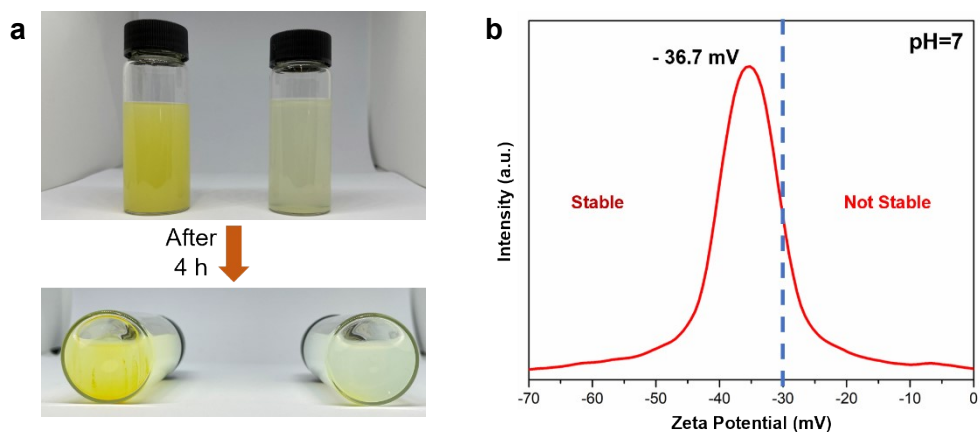


**Fig. S4** (a) Dispersion of FZIS and LZIS-4 in water with a concentration of  $0.5 \text{ g L}^{-1}$ . (b) Zeta potential of LZIS-4 suspension.

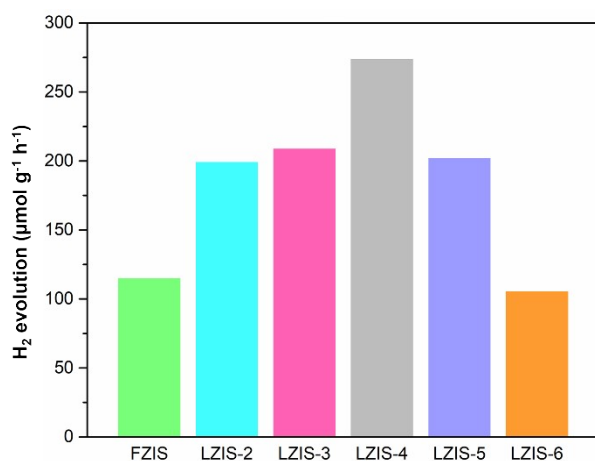


**Fig. S5** H<sub>2</sub> evolution rate of ZnIn<sub>2</sub>S<sub>4</sub> samples in 1 vol% benzyl alcohol aqueous solution under  $\lambda > 420 \text{ nm}$  light irradiation after 4 h.

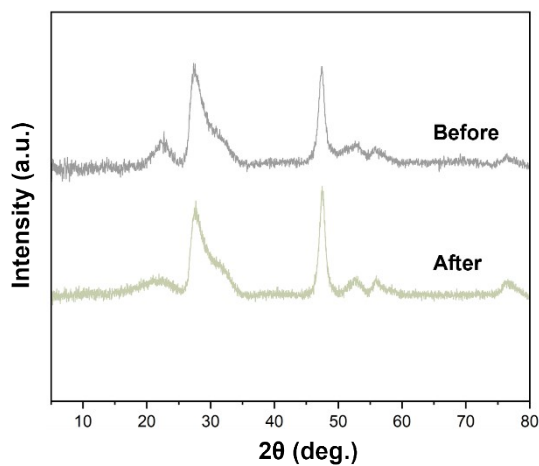


**Fig. S6** XRD patterns of LZIS-4 before and after the prolonged stability (12 h) reaction.

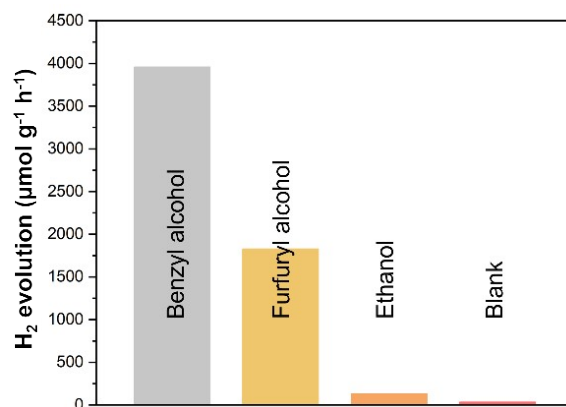


**Fig. S7** Photoredox coupling H<sub>2</sub> evolution rates using different alcohols over LZIS-4. A control set was performed in the absence of alcohols.

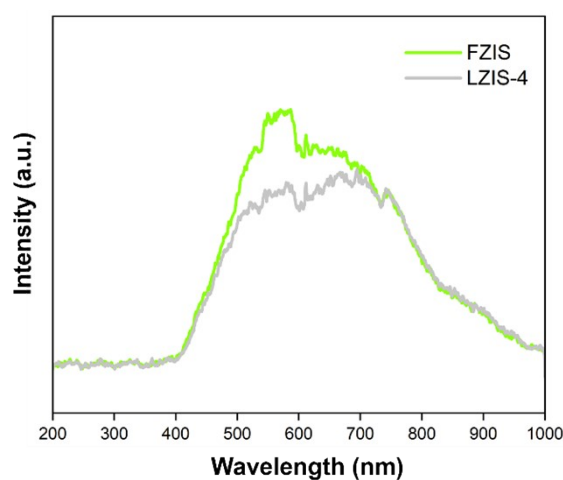


**Fig. S8** Steady-state photoluminescence (PL) spectra of FZIS and LZIS-4.

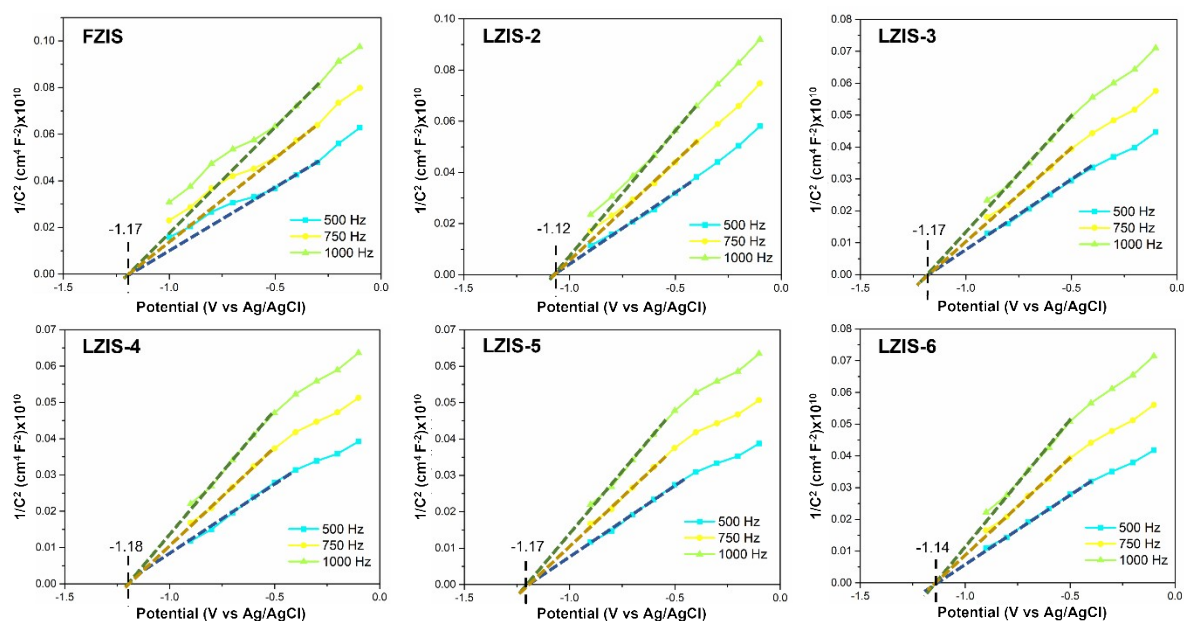


**Fig. S9** Mott-Schottky of ZnIn<sub>2</sub>S<sub>4</sub> samples at frequencies of 500, 750 and 1000 Hz.

**Table S1** Physical properties of the ZIS samples.

<b>Samples</b>	<b>S<sub>BET</sub> (m<sup>2</sup> g<sup>-1</sup>)<sup>a</sup></b>
FZIS	60.18
LZIS-3	66.30
LZIS-4	132.36
LZIS-6	55.59

<sup>a</sup> obtained from BET method

**Table S2** H<sub>2</sub> evolution of LZIS-4 using different bandpass light filters after 4 h.

<b>Wavelength (nm)</b>	<b>H<sub>2</sub> evolution (μmol g<sup>-1</sup> h<sup>-1</sup>)</b>	<b>Light intensity (mW cm<sup>-2</sup>)</b>	<b>AQE (%)</b>
380	1281.95	2.5	5.409
400	733.04	3.1	2.370
420	125.43	3.5	0.342
450	42.003	3.8	0.098
500	3.395	4.1	0.007
550	15.535	4.2	0.027

**Table S3** Comparison of recently reported photocatalytic system in H<sub>2</sub> coupled with selective benzyl alcohol oxidation to benzaldehyde.

Photocatalyst	Light irradiation	Reaction medium	BA conc. (mol L <sup>-1</sup> )	Reaction condition	Duration (h)	HER rate (mmol g <sup>-1</sup> h <sup>-1</sup> )	Benzyl alcohol conversion (%)	Selectivity toward benzaldehyde (%)	Ref
ZnS@Ni <sub>x</sub> S <sub>y</sub>	λ > 200 nm	H <sub>2</sub> O	0.005	N <sub>2</sub>	3	3.65	49.3	80.4	2
Ni-ZIS	λ > 420 nm	H <sub>2</sub> O	0.010	N <sub>2</sub>	5	1.46	97.2	92.8	3
CdS/MIL-53(Fe)	λ > 420 nm	CH <sub>3</sub> CN	0.100	Ar	Not mentioned	2.33	2825 μmol g <sup>-1</sup> h <sup>-1</sup>	99	4
Pt@N vacancies-g-C <sub>3</sub> N <sub>4</sub>	λ > 420 nm	H <sub>2</sub> O	0.100	-	5	0.20	0.50 <sup>a</sup>	98	5
Pt@g-C <sub>3</sub> N <sub>4</sub>	λ > 400 nm	H <sub>2</sub> O	0.010	Ar	20	0.26	40	90	6
polyoxometalate (POM)@ZnIn <sub>2</sub> S <sub>4</sub>	λ > 420 nm	H <sub>2</sub> O	0.020	Ar	5	10.6	96.1	98.2	7
CdS@MoS <sub>2</sub>	λ > 420 nm	CH <sub>3</sub> CN	0.033	Ar	11	2.36	94	99	8
Pt@C-modified g-C <sub>3</sub> N <sub>4</sub>	λ > 420 nm	H <sub>2</sub> O	0.010	-	20	0.29	11.5 <sup>a</sup>	-	9
Ni <sub>12</sub> P <sub>5</sub> @O-ZnIn <sub>2</sub> S <sub>4</sub>	320 nm < λ < 780 nm	H <sub>2</sub> O	0.097	-	3	15.79	16.4 <sup>a</sup>	-	10
S-g-C <sub>3</sub> N <sub>4</sub>	λ > 420 nm	H <sub>2</sub> O	0.010	-	12	0.37	25.1	91.5	11
Mn <sub>0.25</sub> Cd <sub>0.75</sub> S@WO <sub>3</sub>	λ > 420 nm	benzotrifluoride	0.242	Ar	5	4.68	15.9	-	12
CeO <sub>2</sub> /ZnIn <sub>2</sub> S <sub>4</sub>	AM 1.5	CH <sub>3</sub> CN	0.097	Anaerobic	3	1.50	12.4 <sup>a</sup>	96	13
Pt@Pyrimidine-CCN	AM 1.5	H <sub>2</sub> O	0.122	Ar	12	7.47	91	99	14
Cs <sub>2</sub> AgBiBr <sub>6</sub> /TiO <sub>2</sub>	AM 1.5	cyclohexane	0.020	N <sub>2</sub>	8	0.57	75.39	99	15
LZIS-4	AM 1.5	H <sub>2</sub> O	0.097	N <sub>2</sub>	4	3.96	23	96	This work

<sup>a</sup> benzyl alcohol conversion was calculated based on the percentage of then final yield of benzaldehyde (mol) divided by the initial benzyl alcohol added (mol)

**Table S4** Charge resistance of the ZnIn<sub>2</sub>S<sub>4</sub> samples under AM1.5 light on/off condition.

<b>Sample</b>	<b>Light-off R<sub>p</sub> (MΩ)</b>	<b>Light-on R<sub>p</sub> (kΩ)</b>
FIZS	4.64	636
LZIS-2	7.52	397
LZIS-3	2.48	192
LZIS-4	2.24	129
LZIS-5	2.57	206
LZIS-6	6.87	207

**Table S5** Calculated density charge carrier based on Mott-Schottky slope.

<b>Sample</b>	<b>Density of charge carrier (cm<sup>-3</sup>)</b>
FIZS	$7.66 \times 10^{21}$
LZIS-2	$9.05 \times 10^{21}$
LZIS-3	$1.10 \times 10^{22}$
LZIS-4	$1.17 \times 10^{22}$
LZIS-5	$1.15 \times 10^{22}$
LZIS-6	$1.06 \times 10^{22}$

## References

1. X. Ye, T. Zhu, Z. Hui, X. Wang, J. Wei and S. Chen, *J. Catal.*, 2021, **401**, 149-159.
2. H. Hao, L. Zhang, W. Wang, S. Qiao and X. Liu, *ACS Sustain Chem. Eng.*, 2019, **7**, 10501-10508.
3. Q. Lin, Y.-H. Li, M.-Y. Qi, J.-Y. Li, Z.-R. Tang, M. Anpo, Y. M. A. Yamada and Y.-J. Xu, *Appl. Catal., B*, 2020, **271**, 118946.
4. P. Li, X. Yan, S. Gao and R. Cao, *Chem. Eng. J.*, 2021, **421**, 129870.
5. X. Liu, Q. Zhang, Z. Cui, F. Ma, Y. Guo, Z. Wang, Y. Liu, Z. Zheng, H. Cheng, Y. Dai, B. Huang and P. Wang, *Int. J. Hydrogen Energy*, 2022, **47**, 18738-18747.
6. F. Li, Y. Wang, J. Du, Y. Zhu, C. Xu and L. Sun, *Appl. Catal., B*, 2018, **225**, 258-263.
7. F. Xing, R. Zeng, C. Cheng, Q. Liu and C. Huang, *Appl. Catal., B*, 2022, **306**, 121087.
8. P. Li, H. Zhao, X. Yan, X. Yang, J. Li, S. Gao and R. Cao, *Sci. China Mater.*, 2020, **63**, 2239-2250.
9. H. Wang, J. Zhang, X. Jin, X. Wang, F. Zhang, J. Xue, Y. Li, J. Li and G. Zhang, *J. Mater. Chem. A*, 2021, **9**, 7143-7149.
10. J. Wan, L. Liu, Y. Wu, J. Song, J. Liu, R. Song, J. Low, X. Chen, J. Wang, F. Fu and Y. Xiong, *Adv. Funct. Mater.*, 2022, **32**, 2203252.
11. F. Zhang, J. Li, H. Wang, Y. Li, Y. Liu, Q. Qian, X. Jin, X. Wang, J. Zhang and G. Zhang, *Appl. Catal., B*, 2020, **269**, 118772.
12. J. Wang, Y. Zhang, X. Wang and W. Su, *Appl. Catal., B*, 2020, **268**, 118444.
13. C. Jiang, H. Wang, Y. Wang and H. Ji, *Appl. Catal., B*, 2020, **277**, 119235.
14. Z. Lin, Y. Wang, T. Thi Thuy Nga, J. Zhang, R. Wang, Z. Zhang, Y. Xu, D. Zhao, C.-L. Dong and S. Shen, *EES Catalysis*, 2023, DOI: 10.1039/D3EY00055A.
15. M. Yu, N. Wang, K. Lin, D. Song, J. Chen, T. Liang, J. Sun, K. Pan and H. Fu, *J. Mater. Chem. A*, 2023, **11**, 4302-4309.